Observed estimates of convergence in the Savu Sea, Indonesia

James T. Potemra,[1] Janet Sprintall,[2] Susan L. Hautala,[3] and Wahyu Pandoe[4,5]

Received 11 June 2002; revised 25 September 2002; accepted 10 October 2002; published 2 January 2003.

[1] The Indonesian seas are known to be a region where various Pacific and Indian Ocean water masses converge and are transformed into uniquely characterized Indonesian Sea Water (ISW). The volume of Pacific surface waters that are stored in the Indonesian seas and the timescales for this volume to change are important factors in the formulation of ISW that ultimately enters the Indian Ocean as the Indonesian throughflow (ITF). In this study, data from a recent deployment of pressure gauges surrounding the Savu Sea are used to estimate volume, heat, and freshwater convergence within approximately the upper 100 m. A pair of gauges on the northeastern side (North Ombai and South Ombai) is used to estimate inflow from the Banda Sea through the Ombai Strait, and two pairs (Sumbawa/North Sumba and South Sumba/Roti) are used to estimate outflow to the Indian Ocean via the Sumba and Savu/Dao Straits. The data are used in conjunction with numerical model results to show that at times, for example, November and December of 1996, there can be up to a 10 Sv imbalance between the inflow and the outflow transport. Most of the variability in estimated convergence occurs intraseasonally and seems to be controlled by the flow through the Sumba Strait on the eastern side of the sea. The annual cycle of convergence is smaller and ranges from 4 Sv in December through February to −2 Sv (divergence) in August through October. Lower-frequency variations based on model results are consistent with satellite derived sea level and sea surface temperatures in the Savu Sea and show that during recent El Niño-Southern Oscillation events there is anomalous heat divergence (convergence) in the Savu Sea during El Niños (La Niñas). *INDEX TERMS:* 4532 Oceanography: Physical: General circulation; 4572 Oceanography: Physical: Upper ocean processes; 4279 Oceanography: General: Upwelling and convergences; *KEYWORDS:* Indonesian throughflow, Savu Sea

Citation: Potemra, J. T., J. Sprintall, S. L. Hautala, and W. Pandoe, Observed estimates of convergence in the Savu Sea, Indonesia, *J. Geophys. Res.*, *108*(C1), 3001, doi:10.1029/2002JC001507, 2003.

1. Introduction

[2] Recent estimates of Indonesian throughflow (ITF) transport based on in situ observations suggest a phase difference between the inflow transport from the Pacific [*Gordon et al.*, 1999] and the outflow transport to the Indian Ocean [*Hautala et al.*, 2001] on various timescales. For example, while measured flow through Makassar Strait (an entry strait to the Indonesian seas) was high during the NW monsoon of 1996–1997 [*Gordon et al.*, 1999], flow though the exit passages was low [*Hautala et al.*, 2001]. These estimates, however, are based on different types of measurements and depth ranges. Unfortunately, due to a lack of observations, a comprehensive analysis cannot yet be made over the entire Indonesian seas. Here, however, we use consistent measurements of both the inflow and outflow sides of one internal Indonesian sea, the Savu Sea, to study mass, heat and freshwater convergence in the upper layer of the sea.

[3] Simultaneous observations of pressure (P), temperature (T), and salinity (s) in the straits that enclose the Savu Sea (Figure 1), i.e., Ombai Strait on the eastern edge, Sumba Strait on the western edge, and Savu/Dao Straits to the south, form the basis for our study. The observations were made using gauges initiated and maintained as part of the three year (1995–1998) Shallow Pressure Gauge Array (SPGA) study. The bottom-mounted pressure gauges, located at approximately 10 m depth, were designed to obtain an estimate of the horizontally averaged, surface geostrophic flow through five passages in the Lesser Sunda Islands known collectively as Nusa Tengarra [*Chong et al.*, 2000]. Details and results of the SPGA have been described by *Chong et al.* [2000], *Hautala et al.* [2001], *Potemra et al.* [2002a], and *Sprintall et al.* [2002]. Meas-

[1]International Pacific Research Center, School of Ocean and Earth Science and Technology, University of Hawaii, Honolulu, Hawaii, USA.
[2]Physical Oceanography Research Division, Scripps Institution of Oceanography, University of California, San Diego, La Jolla, California, USA.
[3]School of Oceanography, University of Washington, Seattle, Washington, USA.
[4]Department of Oceanography, Texas A&M University, College Station, Texas, USA.
[5]Also at Agency for the Assessment and Application of Technology, Jakarta, Indonesia.

0148-0227/03/2002JC001507$09.00

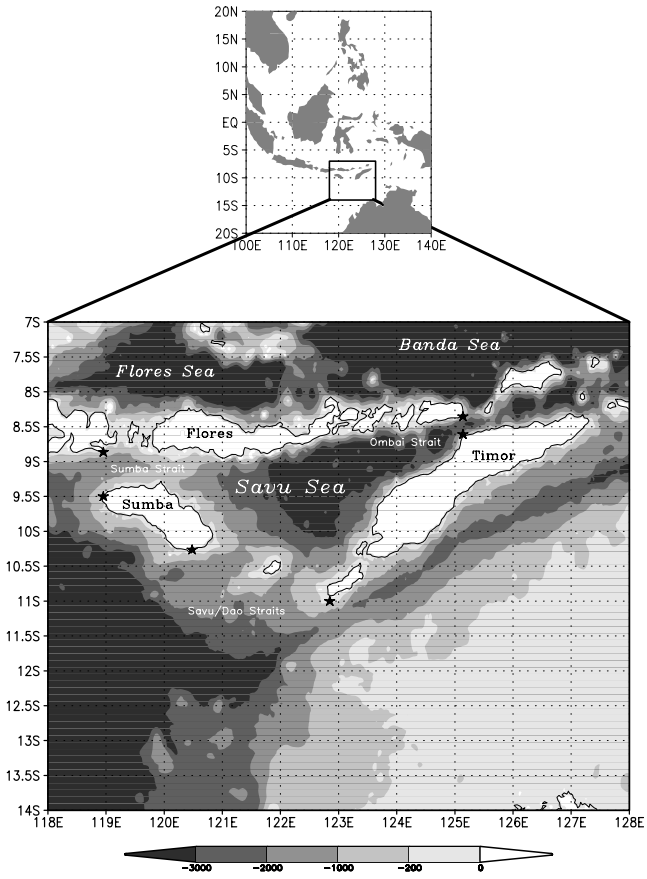

Figure 1. A map of the Indonesian seas is given, with a focus on (bottom) the Savu Sea. Bathymetry from *Smith and Sandwell* [1997] is shaded, and the locations of the gauges are given with stars.

urements were collected across the Sumba Strait at Sumbawa on the northern side and North Sumba on the southern side. The depth between these two stations reaches 1500 m, but there is a shallow sill to the east, within the Savu Sea, of about 350 m. The Ombai Strait, measured at North Ombai on the northern side and South Ombai on the southern side, is 2700 m deep between the gauges. To the northeast is a slightly more shallow sill of 1800 m. The Savu/Dao Straits were measured as one, with a gauge at South Sumba on the northern side and at a gauge at Roti on the southern side. The Savu Strait is the deeper of the two, approximately 1500 m, compared to Dao at 1200 m.

[4] A numerical model, validated to a certain degree with the observations, is used to estimate the vertical structure of the transport. Given the nature of the measurements, we restrict our analysis to the baroclinic nature of the flow, and focus on convergence of water in a upper layer, approximately the upper 100 m.

[5] The Savu Sea is to the south of the large, internal Indonesian Banda and Flores Seas (Figure 1). The region is subject to seasonally reversing monsoon winds (Figure 2) that are from the southeast in austral winter (April through November) and from the northwest in austral summer (December through March). These winds contribute to the transport of upper ocean waters from the Pacific to the Indian Ocean, the ITF, which is maximum during the SE monsoon and minimum during the NW monsoon [*Wyrtki*, 1961].

[6] Observations [*Hautala et al.*, 2001] and previous modeling work [e.g., *Potemra et al.*, 2002b] suggest that the major variations in flow through the Indonesian passages occurs in two layers; a surface intensified layer to 100 m and a layer from 100 to about 500 m. The *Levitus and Boyer* [1994] and *Levitus et al.* [1994] analysis of temperature and salinity observations in the Savu Sea does not show a clear mixed layer in the annual mean, but the maximum change in density with depth occurs at 75 m. Surface temperatures average slightly above 28°C, and decay to 7.5°C at 500 m. Salinity is low in the surface levels (34.1) and increases to a maximum of 34.55 at 200 m.

[7] Ekman pumping velocity, $\frac{1}{\rho}\nabla \times \frac{\tau}{f}$, computed from the ECMWF surface wind fields is shown in Figure 2b for the Savu Sea. Cooling from coastal upwelling also occurs in the Savu Sea, but since the Savu Sea is mostly closed, upwelling conditions on one side of the sea should be mostly countered by downwelling conditions on the opposite side. Wind stress in the interior of the Savu Sea provides upwelling via Ekman pumping throughout the year, with a maximum around 0.35 m d^{-1} in June and July, compared to the annual mean of 0.15 m d^{-1} (Figure 2). This translates to a heat flux of approximately 7.1 ΔT W m^{-2} across the base of the mixed layer, where ΔT is the difference between the temperature of the mixed layer and the layer below. In section 4 we use in situ observations of temperature to derive a more accurate estimate of the potential heat flux due to upwelling.

[8] The seasonal mean surface air-sea heat flux over the Savu Sea is semiannual, driven mainly by the semiannual changes in incoming solar radiation, but there is also a semiannual signal in the longwave and sensible heat fluxes (Figure 3). The air-sea heat flux is minimum during the SE monsoon, especially in June and July. On average, air-sea heat fluxes provide 53 W m^{-2} heating to the ocean surface, with local maxima of 80 W m^{-2} in March and over 100 W m^{-2} in October.

[9] An interesting, complex balance therefore exists in the upper wind-driven layer of the Savu Sea between the air-sea heat flux that heats the upper layer on semiannual timescales and vertical advection at the base of the wind driven layer due to Ekman pumping that cools the upper layer on annual timescales.

[10] Another contribution to be considered in the heat balance of the Savu Sea are changes due to convergence of transport within the sea. This can be estimated through the differences in inflow and outflow transport estimated from the pressure gauges that surround the Savu Sea. Short-term changes due to tides are no doubt important as well, but our observations cannot address these, and we will instead focus on seasonal to interannual changes. In general, the ITF is maximum toward the Indian Ocean during the SE monsoon and carries warm, fresh water in the near surface layer [*Chong et al.*, 2000]. Hence the strong ITF in austral winter coincides with minimum surface heating from the net air-sea heat flux (Figure 3) and maximum upwelling from Ekman pumping (Figure 2). How do these three factors combine to affect upper ocean

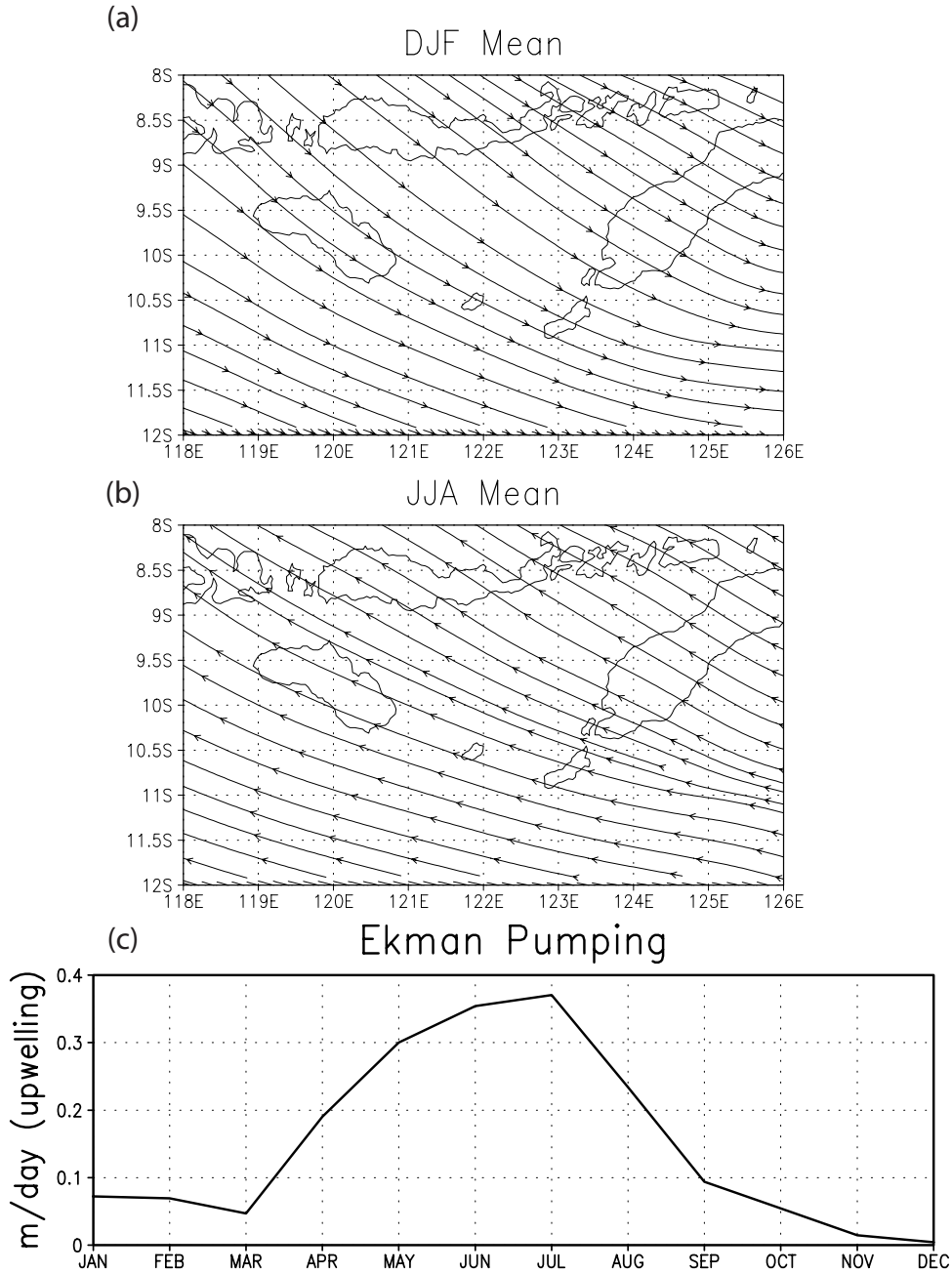

Figure 2. Mean surface winds from ECMWF are shown for the (a) NW monsoon (December, January, and February) and for the (b) SE monsoon (June, July, and August). (c) Ekman pumping, computed from the same ECMWF climatology, is averaged over the Savu Sea interior (121°–123°E, 10°–9°S).

heat content in the Savu Sea? This is the central focus of our study.

2. Components of the Heat Balance in the Savu Sea

[11] We write the change in heat in the upper layer, z_o, of the Savu Sea as

$$\underbrace{z_o \mathcal{A} \rho C_P \frac{\partial T}{\partial t}}_{1} = \underbrace{\mathcal{A} \rho C_P w_{z_o} T_{z_o}}_{2} + \underbrace{\rho C_P \sum V_{in} T_{in}}_{3} + \underbrace{\mathcal{A} Q_{net}}_{4} \quad (1)$$

where,

1 Heat change over time;
2 Change in heat due to vertical motions;
3 Change in heat due to transport convergence;
4 Change in heat due to surface air-sea heat fluxes.

[12] The vertical velocity, w_{z_o} (term 2) is the sum of Ekman upwelling (that exits the sea through one or more of the straits) and any externally driven upper layer strait flow convergence. The transport convergence (term 3) is the sum of the upper layer transport times the upper layer temperature through each of the three straits that surround the Savu Sea (this will be estimated in section 4). Equation (1) can

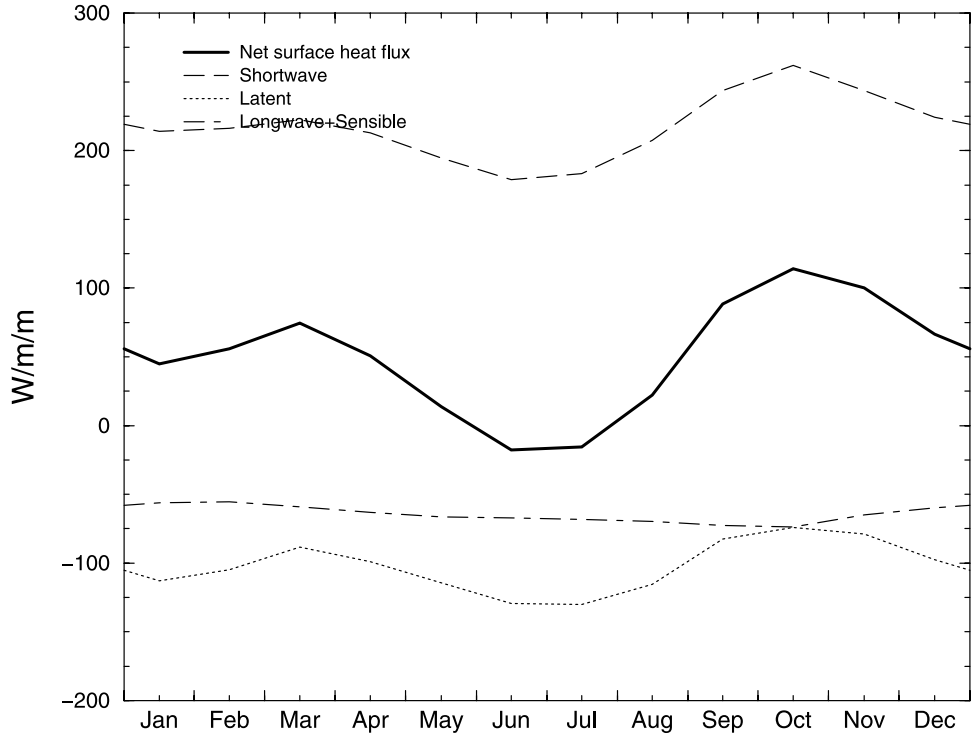

Figure 3. Seasonal mean surface heat fluxes from NCEP averaged over the Savu Sea (119°–125°E, 10.5°–9°S). The net surface heat flux is given with the heavy line. Positive indicates heating at the ocean surface.

thus be written

$$z_o \mathcal{A}\rho C_P \frac{\partial T}{\partial t} = \mathcal{A}\rho C_P w_{z_o}(t) T_{z_o}(t) + \rho C_P[-V_{ombai}(t)T_{ombai}(t) + V_{sumba}(t)T_{sumba}(t) + V_{savu}(t)T_{savu}(t)] + \mathcal{A}Q_{net}(t). \quad (2)$$

[13] In this formulation, we are neglecting the effects of eddy dissipation, which are assumed to be small, and the effects of entrainment due to turbulence at the base of the mixed layer. A typical parameterization of the entrainment heat flux, based on the friction velocity of the wind, shows this term to be an order of magnitude less than the others (based on mean ECMWF wind speeds in the sea). We further assume that the area of the upper layer does not change; the specific heat (C_P), density (ρ), and the area of the upper layer ($\mathcal{A}$) are taken to be constants of 3994 J kg^{-1}°C^{-1}, 1024 kg m^{-3}, and 8×10^{10} m^2, respectively. It should also be noted that vertical motions of the upper layer are assumed to be controlled in the sea by Ekman pumping or divergence of the inflow and outflow; divergence of flow within the sea itself, and Ekman flow in the straits are neglected.

[14] The upper layer transports can be estimated from 3-day averaged observations of cross-strait pressure difference (e.g., V_{sumba} is obtained from $\eta_{sumbawa} - \eta_{n.\ sumba}$) from the SPGA gauges. To extrapolate these measurements to values over the upper layer, a numerical model is used to derive a relationship between surface and depth-integrated values. In the following section, model sea level at the SGPA sites is compared to the observations. A linear relationship between model sea level and model transport is then found. This relationship is then applied to the observed sea level to estimate transport through the straits. Storage in the upper ocean is then computed as a balance of the inflow and outflow transport. Near surface temperature in the straits comes from collocated temperature sensors at the pressure gauge sites, and these values are used to represent the mean over the upper layer. In section 4 the observed temperature and salinity data are used to estimate the heat and freshwater balance within the Savu Sea.

3. Estimated Volume Storage

[15] The in situ gauges measure pressure at each side of the Ombai, Sumba and Savu/Dao Straits. The pressure difference across each strait can be used to estimate surface geostrophic velocity through the strait via $\frac{g}{f}\frac{\Delta\eta}{\Delta x}$, where $\Delta\eta$ is the pressure difference, Δx is the cross strait distance, and $\frac{g}{f}$ is gravity over the Coriolis parameter. Since we have limited observations within the straits, the challenge is to obtain a depth integrated transport from this surface geostrophic velocity estimate. To accomplish this, we use the results of a numerical model. This method was used by *Potemra et al.* [2002a] for the Ombai, Timor and Lombok Straits. Using this method, it was shown that flow through these straits was in geostrophic balance, and that cross-strait pressure differences could accurately be used to estimate flow down to about 260 m.

[16] The large-scale numerical model used in the present study of the Savu Sea is described by *Potemra et al.* [2002a] and *Potemra et al.* [2002b]. Briefly, the model is a 2-1/2 layer, reduced gravity model. The only forcing is from 3-day ECMWF wind stress (same winds described in the

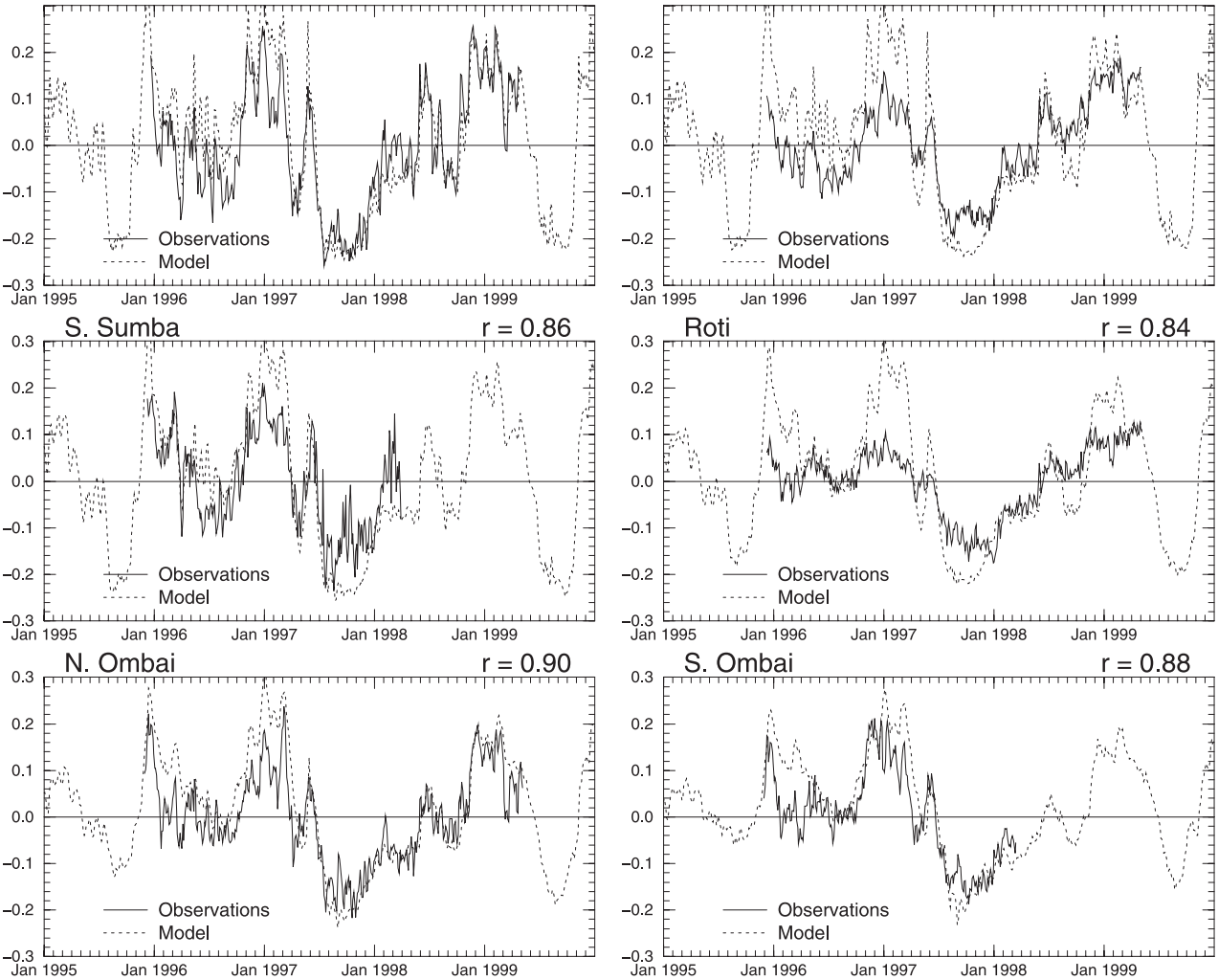

Figure 4. Sea level, in meters, is given from the observations (solid line) and the model (dashed line): (top) for both sides of the Sumba Strait, (middle) for the Savu/Dao Straits, and (bottom) for the Ombai Strait. The long-term mean has been removed from each record. The correlations between the observations and the model results are given in the upper right corner of each panel.

previous section). The model's upper layer is initially 100 m, set to approximate the upper layer flows in the large-scale region of the Indonesian seas.

[17] Figure 4 shows the comparison of sea level from the model and sea level measured by the pressure gauges at the six sites that surround the Savu Sea. In each case the long-term mean has been removed. The model overestimates the observed sea level variations at all the gauge locations, particularly at Roti. Nevertheless, there is a high correlation between the model variations and observations (correlation coefficients range from 0.84 to 0.90), and the model results are only used to estimate transport variations and not total transport.

[18] As a further check on the model, sea level variations within the Savu Sea from the model are compared to sea level variations from the TOPEX/Poseidon (T/P) altimeter in Figure 5. There is a crossover point of the altimeter near the center of the sea (at 9.75°S, 122°E), and model sea level variations, averaged over the interior of the sea, match the T/P remote observations remarkably well ($r = 0.84$). The T/P data, as well as the in situ gauges, show that sea level in the Savu Sea is reduced during the SE monsoon, when net ITF transport is high. As will be shown later, the low sea level is due to upper layer divergence in the Savu Sea.

[19] A multiple linear regression fit was used to determine the relationship of sea level at the sides of a strait to upper layer transport through the strait using the model results. The fit of model transport to sea level at each side, rather than to the cross-strait sea level difference, was made so there was no a priori assumption of geostrophic balance. As it turns out, however, the correlation of model sea level variations to model transport was maximum when the model sea level variations on each side of a strait were weighed by equal magnitudes and opposite sign; in other words, a scaled cross-strait difference in model sea level has the highest correlation to model upper layer transport in that strait. (Figure 6). The model upper layer thickness is about 100 m through these straits, so the result is limited to upper ocean transport only, but previous model experiments have shown that most of the ITF transport through the outflow straits occurs in this upper layer *Potemra et al.*, 2002b].

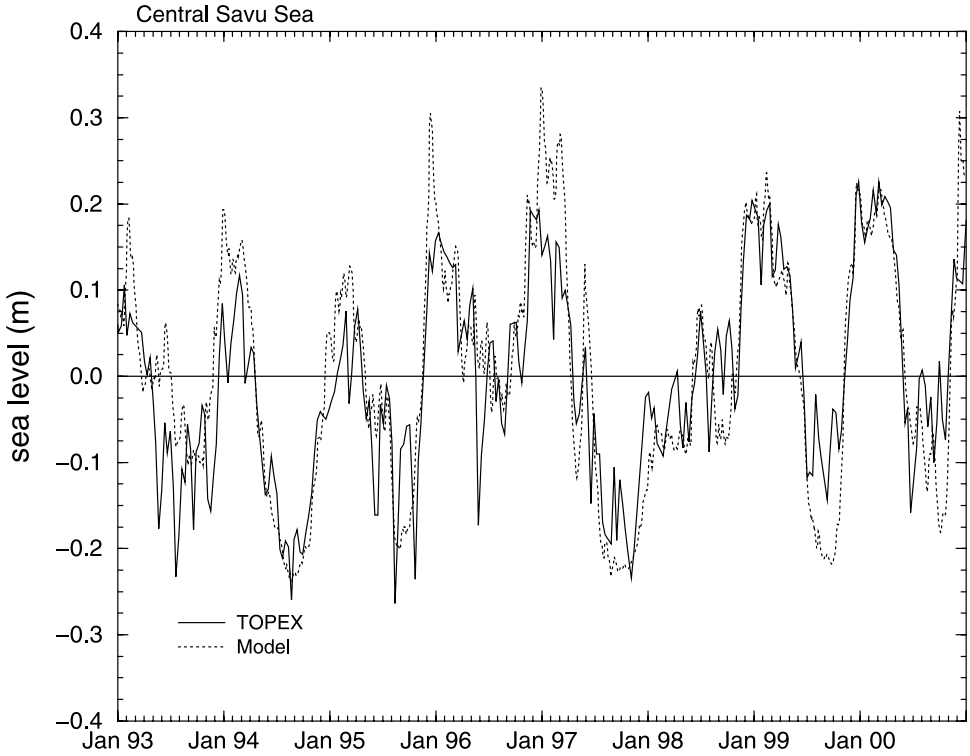

Figure 5. Mean sea level, in meters, over the Savu Sea (121°–124°E, 10.5°–9°S) from the model (dashed line) is compared to sea level from a TOPEX/Poseidon crossover point at the center of the sea. The long-term mean has been removed from each record.

[20] The result of the model analysis gives the following relationship between upper layer (approximately the top 100 m) transport variations, V'_{100} (in sverdrups), and sea level variations, η' (in meters), at each strait:

$$\begin{aligned} V'^{\,Sumba}_{100} &= 39.14\left(\eta'_{sumbawa} - \eta'_{n.sumba}\right) \\ V'^{\,Savu}_{100} &= 27.71\left(\eta'_{s.sumba} - \eta'_{roti}\right) \\ V'^{\,Ombai}_{100} &= 24.08\left(\eta'_{n.ombai} - \eta'_{s.ombai}\right). \end{aligned} \tag{3}$$

[21] Application of the above relationships to the observed pressure differences gives us an estimate for transport in the upper layer. It should be noted that the above relationships are for an active upper layer. The model upper layer in the Savu Sea varies from 80 m in September and October to 115 m in January and February. The annual mean is about 100 m, so that number will be used henceforth to denote this layer. The correlations of the fit to transport are high, 0.92 for Ombai, 0.89 for Savu/Dao and 0.87 for Sumba. The standard error for each is 0.23, 0.34, and 0.51 (for Ombai, Savu/Dao and Sumba, respectively). Similar regressions were made with quadratic and exponential fits, but neither improved the correlation significantly.

[22] A sum of the inflow ($V'^{Sumba}_{100} + V'^{Savu}_{100} - V'^{Ombai}_{100}$) is an estimate for volume convergence in the upper layer of the Savu Sea (Figure 7). During the SE monsoon, when ITF

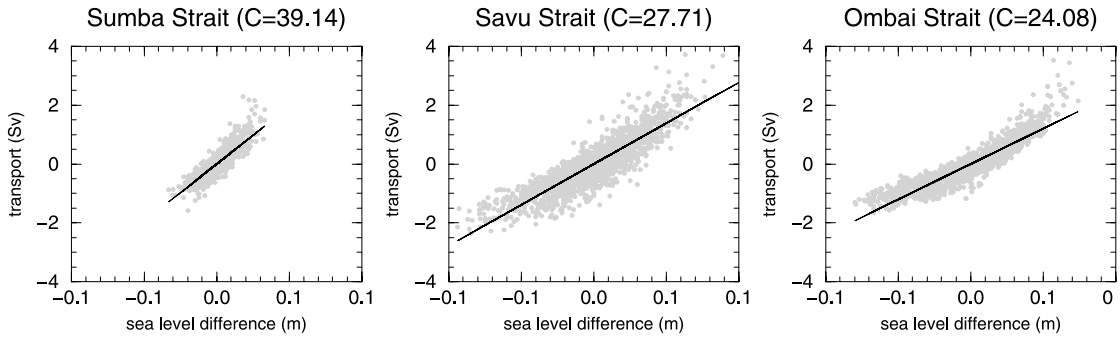

Figure 6. Model upper layer transport variations (in sverdrups) at each strait are plotted as a function of model sea level difference across the strait (in meters). The slope of linear fit, *C*, is given above each panel.

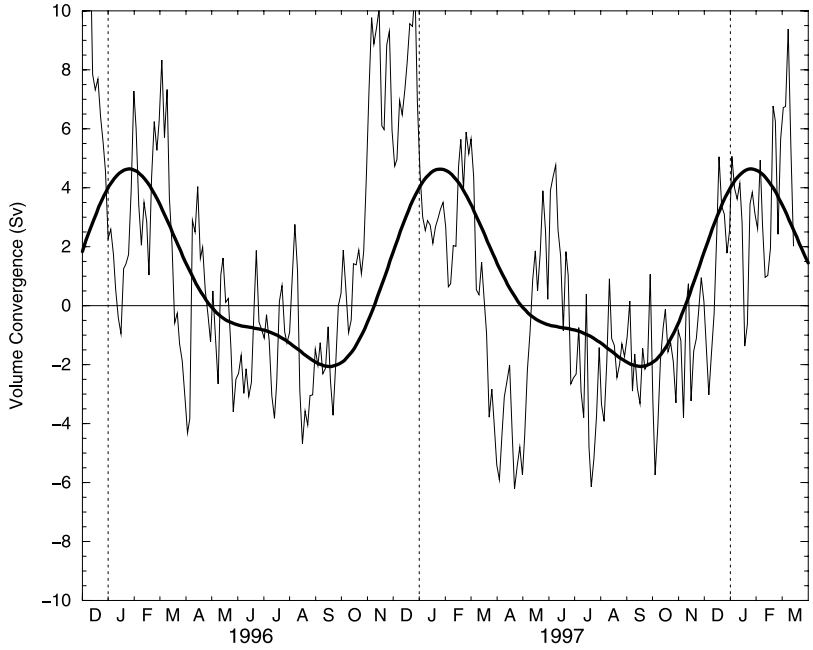

Figure 7. Upper ocean volume convergence in the Savu Sea estimated from the sum of the upper 100 m transport through Ombai, Sumba, and Savu/Dao Straits. The thick line is the annual and semiannual fit of the 3-day measurements. Positive values indicate mass storage in the sea.

transport is high, there is a divergence of mass in the upper layer of the Savu Sea; more mass is leaving the sea than is entering in the upper layer. Upper layer convergence occurs during the NW monsoon, when the net ITF transport is low. The NW monsoon is also a time of minimum upwelling (Figure 2), high SSTs and surface salinities (Figures 8 and 9). We now use the estimates of transport to investigate heat and freshwater fluxes.

4. Heat and Freshwater Fluxes

[23] Transport variations in the upper 100 m of a strait are given by:

$$V'_{100} = \int_0^{100} \int_{x_1}^{x_2} v'(x,z)dx\ dz. \tag{4}$$

[24] We assume an exponential decay with a decay scale α of velocity with depth, $v'(z) = v'_s e^{-\alpha z}$, as supported by various observations [e.g., *Molcard et al.*, 2001; *Hautala et al.*, 2001] and a mean cross-strait geostrophic relation (surface velocity given by v'_s) as indicated by the model, equation (4) may be rewritten:

$$\begin{aligned} V'_{100} &= \int_0^{100} \int_{x_1}^{x_2} v'_s\ e^{-\alpha z}\ dx\ dz \\ &= \frac{g}{f}\left(\frac{1-e^{-100\alpha}}{\alpha}\right)\Delta\eta' \\ &= C\ \Delta\eta'. \end{aligned} \tag{5}$$

[25] Thus, the coefficients obtained in equation (3) can be compared to the coefficient C in equation (5). We further assume that temperature also has an exponential decay with depth (and is also independent of position in the strait): $T(z) = T_s e^{-\beta z}$, where T_s is the measured near-surface temperature. The resulting upper layer heat flux due to transport variations is then given by:

$$\begin{aligned} Q'_{100} &= \rho C_P \Delta x \int_0^{100} v'(z)\ T(z)\ dz \\ &= \rho C_P \Delta x \int_0^{100} v'_s e^{-\alpha z} T_s e^{-\beta z} dz \\ &= \frac{\rho C_P g \Delta\eta' T_s}{f} \int_0^{100} e^{-(\alpha+\beta)z} dz \\ &= \frac{\rho C_P g}{f}\left(\frac{1-e^{-100(\alpha+\beta)}}{\alpha+\beta}\right)\Delta\eta' T_s \end{aligned} \tag{6}$$

A similar expression can be made for the salt flux:

$$\begin{aligned} SF'_{100} &= \frac{\rho}{1000}\Delta x \int_0^{100} v'(z)\ s(z)\ dz \\ &= \frac{\rho}{1000}\Delta x \int_0^{100} v'_s e^{-\alpha z} s_s e^{-\gamma z} dz \\ &= \frac{\rho g \Delta\eta' s_s}{1000 f} \int_0^{100} e^{-(\alpha+\gamma)z} dz \\ &= \frac{\rho g}{1000 f}\left(\frac{1-e^{-100(\alpha+\gamma)}}{\alpha+\gamma}\right)\Delta\eta' s_s \end{aligned} \tag{7}$$

[26] Measurements of temperature and salinity from Savu Sea stations made during the Snellius I expedition were used to derive the decay constants, β and γ (0.0033 and 4.0 $\times$ 10^{-5} m^{-1}, respectively), and the transport to sea level relationship was used to derive α (0.00172, 0.00608, and 0.01433 for Sumba, Savu/Dao and Ombai Straits, respectively). Estimates of heat and freshwater flux are then computed using the observations of $\Delta\eta'$, T, and s from the

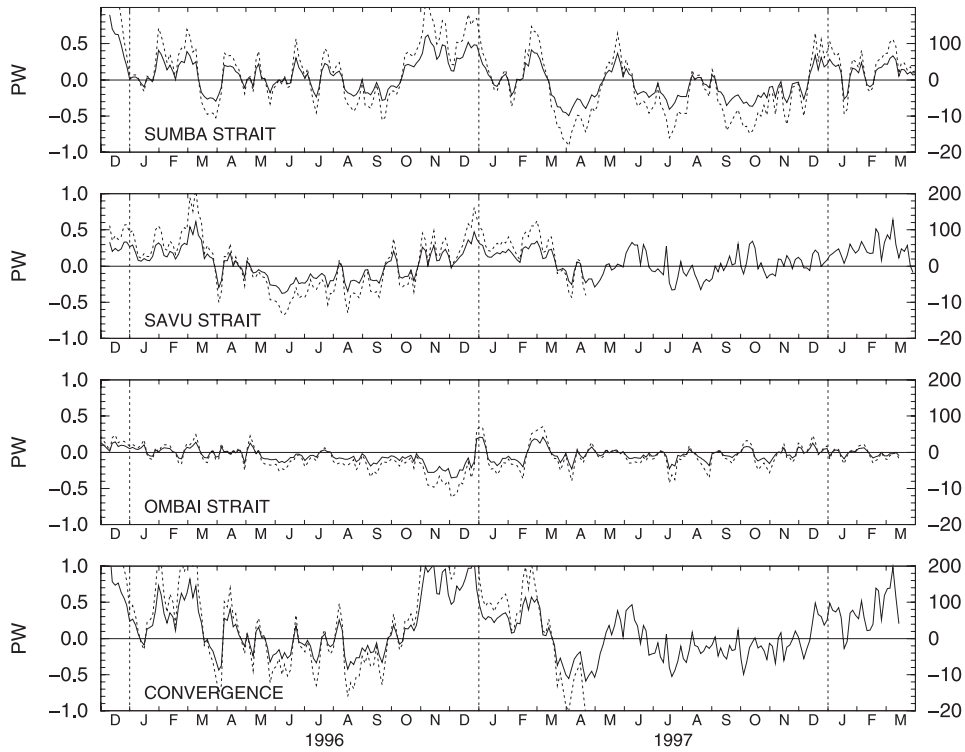

Figure 8. Heat flux estimates from observed cross-strait pressure differences are drawn with the solid lines (scale on the left). Salt flux estimates are drawn with the dotted lines (scale on the right). Negative values indicate an increase in the flux toward the Indian Ocean. (bottom) The convergence of heat/salt in the Savu Sea.

SPGA gauges (Figure 8). The heat flux variations due to transport convergence range from almost −0.5 to 1.0 PW. In comparison, the range in net surface heat flux is 0 to 100 W m^{-2}. When applied to the whole surface area of the Savu Sea, this represents a range of 0 to 8×10^{-3} PW, so the range in heat flux due to transport variations is significantly larger. Salt fluxes are also large, particularly in Sumba and Savu/Dao Straits, ranging from −200 to 200 kT (10^6 kg) of salt per second. For comparison, the surface freshwater flux, estimated by evaporation minus precipitation, ranges from −4 to 4 mm d^{-1}, or an apparent salt flux of about −0.13 to 0.13 kT of salt per second.

[27] The total salt in the upper layer of the Savu Sea ($\bar{s}V\rho_{100}$; mean salinity times the volume times the density of the upper layer) is on order 2.9×10^{14} kg. At a constant flux of 200 kT s^{-1}, the upper layer can be completely flushed in approximately 17 days.

[28] Heat and salt convergence in the Savu Sea due to convergence of flow through the straits is of the same order as the heat and salt fluxes through the inflow/outflow straits; roughly 1 PW of heat gets stored in the sea in austral summer and a net of 0.5 PW is exported from the sea in austral winter (Figure 8). The divergence of heat in austral winter coincides with minimum surface heat fluxes and maximum upwelling from Ekman pumping; all three components of the heat budget act in phase to reduce heat in the Savu Sea during this time. However, the contribution of Ekman pumping to w_{z_o} is small. From Figure 2, maximum Ekman pumping is 0.37 m d^{-1} in July. Assuming this acts over the entire Savu Sea, this represents a transport of approximately 0.34 Sv. Similarly, the contribution of the surface air−sea fluxes (term 4) to changes in upper layer heat content are small compared to the convergence of transport due to flow in the straits. Figure 3 shows a peak air-sea heat flux of 120 W m^{-2} in October, or about 0.01 PW over the entire surface area of the sea.

[29] Various other remote observations in the Savu Sea confirm this seasonal cycle of heat and freshwater fluxes (Figure 9). Primary productivity, measured by SeaWiFS, is maximum in June through September when upwelling due to divergence in flow transport through the straits (and Ekman pumping) is large. SSTs and T/P measured sea level become minimum in August, and precipitation is low.

5. Conclusions

[30] In situ measurements of temperature, salinity and sea surface pressure (sea level) at three straits enclosing the Savu Sea are used to estimate storage within the sea. Since the sea level measurements only resolve surface flow, numerical model results are used to derive a relationship between model sea level, that is highly correlated to observed sea level, and model upper ocean transport. This relationship was then applied to the observed sea level variations to get transport estimates.

[31] Transport convergence estimated in this way is maximum in austral summer, during the NW monsoon, although these estimates of the seasonal cycle are based on only two years of simultaneous observations. Remote

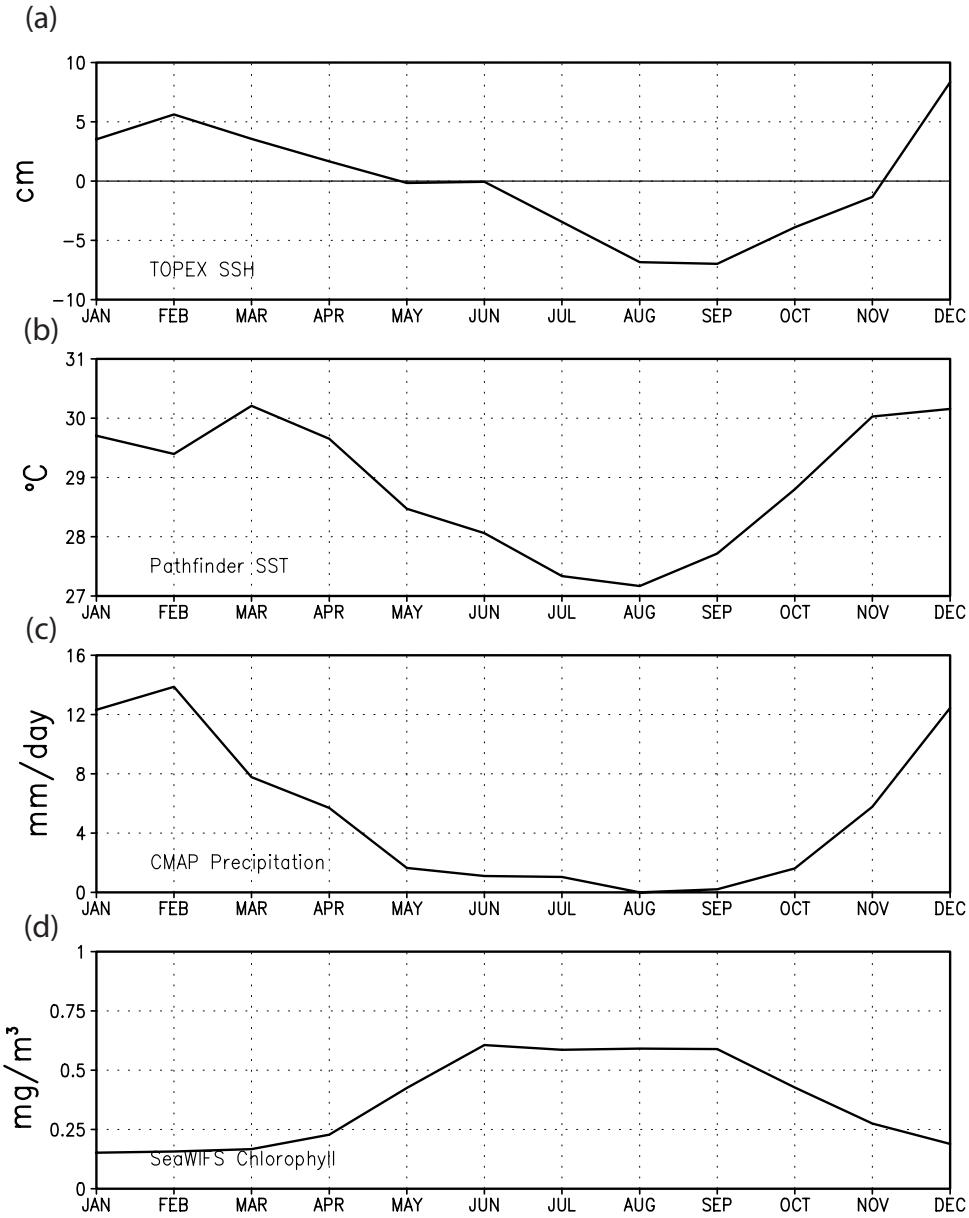

Figure 9. Mean climatological observations averaged over the Savu Sea (121°–123.5°E, 10°–9°S): (a) sea level variations from TOPEX/Poseidon, (b) Pathfinder SST, (c) precipitation from CMAP, and (d) chlorophyll concentration from SeaWiFS.

observations of SST, sea level, chlorophyll, and precipitation along with derived estimates of upwelling from Ekman pumping, give a coherent scenario of the upper layer. Precipitation peaks in February. A month later subsurface salinity is at its minimum. The net surface heating decreases to a minimum in June and upwelling due to Ekman pumping is maximum. Subsequently, SST and subsurface temperature reach a minimum in July/August. Sea level is minimum a month later, when transport is greatest, and there is divergence in the central Savu Sea. These factors combine to cause a peak in productivity (as inferred from the ocean color).

[32] Perhaps more remarkable are the intraseasonal and interannual variability of the transport and mass convergence (Figure 7) in the Savu Sea over the two year period. The observations alone are not sufficient to make conclusions about long-term variations, but the model results (Figure 10), and various remotely sensed observations (Figure 11) can be examined. The long-term model results of convergence in the Savu Sea are similar to the model convergence in the annual cycle, in that warm events mirror the SE Monsoon (Figure 10). During El Niños (e.g., 1997–1998), sea level from T/P is reduced and precipitation from CMAP is reduced (Figure 11). During these same events, model transport increases in the Ombai and Savu Dao Straits, and there is divergence in the upper layer of the Savu Sea. Unlike the annual cycle, however, upwelling becomes anomalously low, and Pathfinder SSTs do not show a correlation to El Niño-Southern Oscillation (ENSO).

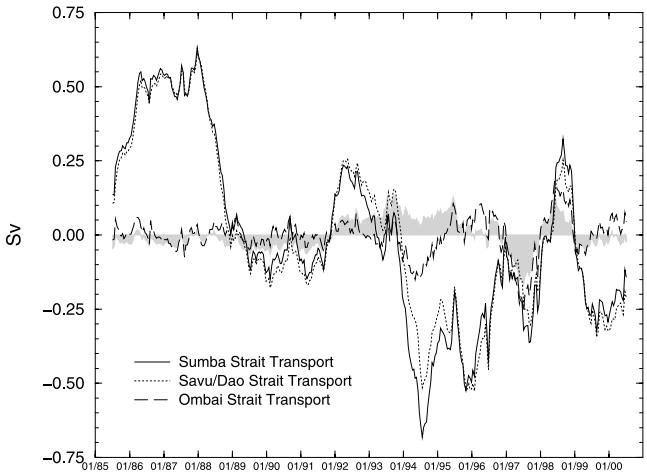

Figure 10. Upper layer transport computed from 3-day model output, fit by a running annual mean filter, is given for each strait. The convergence of upper layer volume is shaded, with positive values indicating convergence.

[33] Finally, the long-term model estimates of convergence in the Savu Sea suggest that upper layer flow through the Ombai Strait is correlated to flow though the Savu/Dao Straits (r = 0.94; Figure 10). Convergence, then, is highly correlated to flow in and out of the Sumba Strait (r = 0.90). This flow through the Sumba Strait is related to the South Java Current [*Sprintall et al.*, 1999]. In March of 1997, when the model shows divergence in the Savu Sea, model upper layer flow is to the west in the Sumba Strait. Conversely in May 1997 there is convergence in the model upper layer, and flow is to the east in the Sumba Strait. This correlation is somewhat confirmed by the observations. Geostrophic flow estimated between South Sumba and North Ombai (Figure 1), computed using the observed pressure difference between South Sumba and North Ombai, is small, suggesting that flow through the Sumba Strait does not exit the Savu/Dao Strait to the south. This has also been suggested through water mass analysis in these straits by *Fieux et al.* [1996].

[34] Having the observations of pressure, temperature and salinity at the three main entrances to the Savu Sea allows us to conjecture about the mass, heat and salt convergence in the sea. However, we are still limited by the depth and temporal range of the observations. To overcome these limitations we rely on a numerical model. Finally, the Savu Sea is one of several major seas within Indonesia. In the future, coordinated efforts at some of the larger of these seas, particularly the Banda Sea, would allow for a more significant estimate of upper ocean fluxes and studies of water mass transformation.

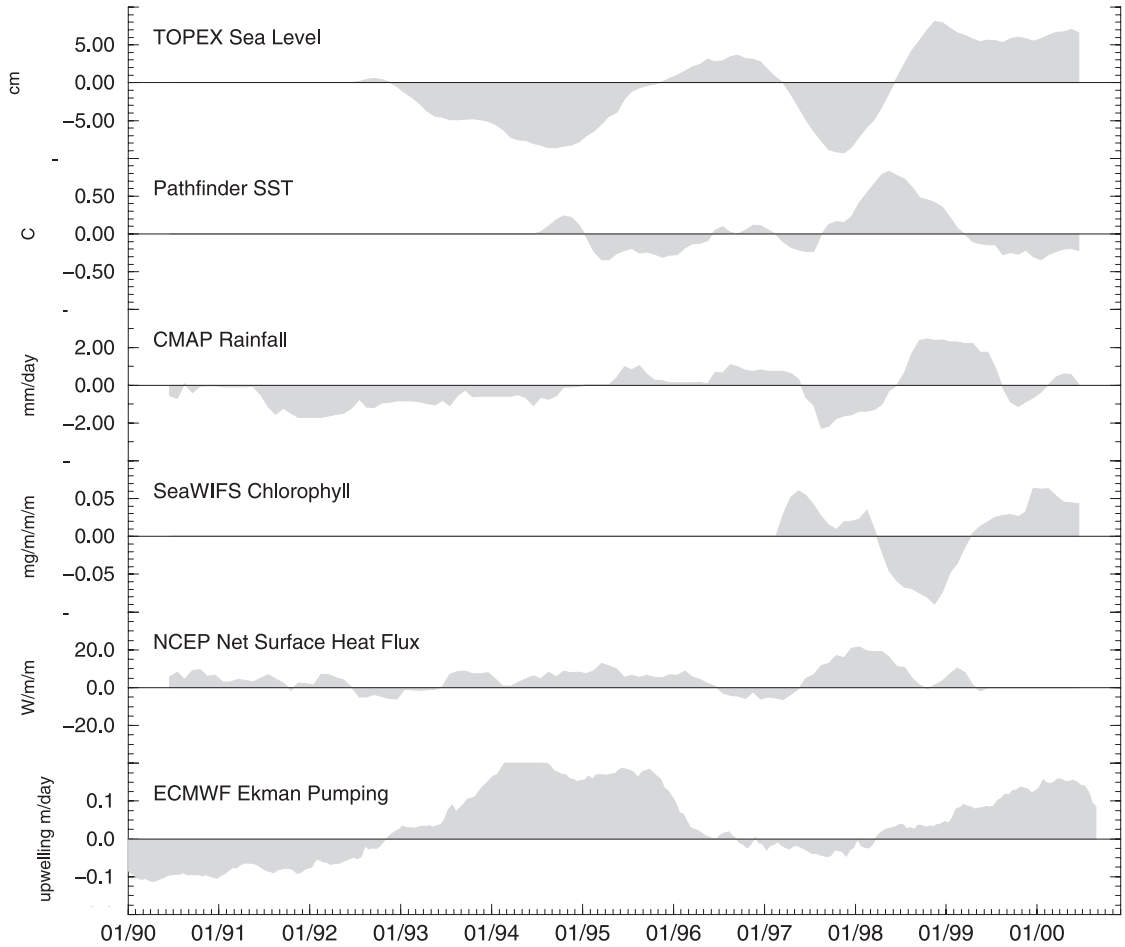

Figure 11. Long-term variations (long-term mean removed) of various parameters over the Savu Sea (mean taken over 121°–123°E, 10°–9°S).

[35] **Acknowledgments.** The success of the Shallow Pressure Gauge Array (SPGA) program that provided the data for this work was due in large part to the efforts of Nan Bray, who, among other things, not only initiated the program but also served as chief scientist on the first two cruises. We also gratefully acknowledge the commanders and crew of the R/V *Baruna Jaya I* and *R/V Baruna Jaya IV* for their capable and enthusiastic support of the project. We also thank our colleagues at BPPT Indonesia, particularly Indroyono Soesilo and Basri Gani, and Gani Ilahude at LIPI for their organizational efforts and warm collegiality. The field support, technical expertise, and scientific insight of Werner Morawitz, Thomas Moore, Paul Harvey, and Jackson Chong were an important part of the program. Financial support was provided by the National Science Foundation (OCE-9819511, OCE-9818670, OCE-9505595, OCE-9415897, and OCE-9529641) and the Office of Naval Research (N00014-94-1-0617). Finally, we thank Robert Molcard, an anonymous reviewer, and the editor John Toole; comments from all greatly improved the manuscript. This research was supported by the Frontier Research System for Global Change through its sponsorship of the International Pacific Research Center. School of Ocean and Earth Science and Technology contribution number 6042 and International Pacific Research Center contribution number IPRC-177.

References

Chong, J. C., J. Sprintall, W. L. M. Morawitz, S. Hautala, N. A. Bray, and W. Pandoe, Transport through the outflow straits of Indonesia, *Geophys. Res. Lett.*, *27*, 125–128, 2000.

Fieux, M., C. Andrie, E. Charriaud, A. G. Ilahude, N. Metzl, R. Molcard, and J. C. Swallow, Hydrological and chlorofluoromethane measurements of the Indonesian throughflow entering the Indian Ocean, *J. Geophys. Res.*, *101*, 12,433–12,454, 1996.

Gordon, A. L., R. D. Susanto, and A. L. Ffield, Throughflow within Makassar Strait, *Geophys. Res. Lett.*, *26*, 3325–3328, 1999.

Hautala, S. L., J. Sprintall, J. T. Potemra, A. G. Ilahude, J. C. Chong, W. Pandoe, and N. Bray, Velocity structure and transport of the Indonesian throughflow in the major straits restricting flow into the Indian Ocean, *J. Geophys. Res.*, *106*, 19,527–19,546, 2001.

Levitus, S., and T. B. Boyer, *World Ocean Atlas 1994*, vol. 4, *Temperature, NOAA Atlas NESDIS*, vol. 4, 129 pp., Natl. Oceanic and Atmos. Admin., Silver Spring, Md., 1994.

Levitus, S., R. Burgett, and T. B. Boyer, *World Ocean Atlas 1994*, vol. 3, *Salinity, NOAA Atlas NESDIS*, vol. 3, 111 pp., Natl. Oceanic and Atmos. Admin., Silver Spring, Md., 1994.

Molcard, R., M. Fieux, and F. Syamsudin, The throughflow within Ombai Strait, *Deep Sea Res., Part I*, *48*, 481,237–481,253, 2001.

Potemra, J. T., S. L. Hautala, J. Sprintall, and W. Pandoe, Interaction between the Indonesian Seas and the Indian Ocean in observations and numerical models, *J. Phys. Oceanogr.*, *32*, 1838–1854, 2002a.

Potemra, J. T., S. L. Hautala, and J. Sprintall, Vertical structure of Indonesian throughflow in a large-scale model, *Deep Sea Res., Part II*, in press, 2002b.

Smith, W. H. F., and D. T. Sandwell, Global seafloor topography from satellite altimetry and ship depth soundings, *Science*, *277*, 1956–1962, 1997.

Sprintall, J., J. Chong, F. Syamsudin, W. Morawitz, S. Hautala, N. Bray, and S. Wijffels, Dynamics of the South Java Current in the Indo-Australian Basin, *Geophys. Res. Lett.*, *26*, 2493–2496, 1999.

Sprintall, J., J. T. Potemra, S. L. Hautala, N. A. Bray, and W. W. Pandoe, Temperature and salinity variability in the exit passages of the Indonesian throughflow, *Deep Sea Res., Part II*, in press, 2002.

Wyrtki, K., Physical oceanography of the southeast Asian waters, *NAGA Rep. 2*, 195 pp., Scripps Inst. of Oceanogr., La Jolla, Calif., 1961.

J. T. Potemra, IPRC/SOEST, University of Hawaii, 2525 Correl Road, Honolulu, HI 96822, USA. (jimp@soest.hawaii.edu)

J. Sprintall, Physical Oceanography Research Division, Scripps Institution of Oceanography, 9500 Gillman Drive, La Jolla, CA 92093-0230, USA. (jsprintall@ucsd.edu)

S. L. Hautala, School of Oceanography, University of Washington, Box 357940, Seattle, WA 98195, USA. (susanh@ocean.washington.edu)

W. Pandoe, Department of Oceanography, O&M Building, Room 602, Texas A&M University, College Station, TX 77843-3146, USA. (wpandoe@ocean.tamu.edu)